Kang, Hyeongsik; Choi, Sung-Uk

Numerical Investigations of the Initiation Mechanism of Cellular Secondary Currents in Open-Channel Flows

NUMERICAL INVESTIGATIONS OF THE INITIATION MECHANISM OF CELLULAR SECONDARY CURRENTS IN OPEN-CHANNEL FLOWS

Hyeongsik Kang[1], Sung-Uk Choi[2]
[1] Research Professor, School of Civil & Environmental Engineering, Yonsei University
Shinchon-dong, Seodaemun-gu, Seoul 120-749, e-mail: kanghs@yonsei.ac.kr
[2] Professor, School of Civil & Environmental Engineering, Yonsei University
Shinchon-dong, Seodaemun-gu, Seoul 120-749, e-mail: schoi@yonsei.ac.kr

ABSTRACT

The initiation mechanism of cellular secondary currents is numerically investigated. The RANS equations in curvilinear coordinates are solved with the non-linear k-ε model. First, the developed model is applied to flows over a fixed sand ridges and troughs in order to check the performance of the model. The simulated results are compared with experimental data available in the literature. The bed elevation changes are simulated in wide rectangular open-channel flows over sand bed by solving the Exner's equation. The simulated results showed that the bottom is firstly eroded near the sidewall due to the corner vortex and the eroded sediment load is transversely transported. Thus, the initial flat bed is gradually deformed and finally becomes ridges and troughs which are called as sand ribbons. The calculated secondary currents clearly showed upflows and downflows over the ridges and troughs, respectively. Changes in bed shear stress and bed elevation with time are also investigated.

Keywords: cellular secondary currents, initiation mechanism, non-linear k-ε model, bed elevation change, sediment transport

1. INTRODUCTION

Many field observations suggested the existence of cellular secondary currents in straight wide rivers. Vanoni (1946) observed a periodic spanwise variation of sediment concentration in a wide open-channel, and he concluded that this phenomenon might be related to the generation of cellular secondary currents. Kinoshita (1967), through aerial stereoscopic survey of a flood flow, noticed that high speed and low speed zones are repeated over the width and that the flows in the low speed zones are laden with high concentrations of sediment. The existence of cellular secondary currents has also been suggested from observations of longitudinal bedforms such as ridges and troughs on the river bed (Karcz,1966; Culberston, 1967; Allen, 1984). The cellular secondary currents are important in hydraulic engineering because they might cause three dimensional sediment transport and bedforms in rivers. Despite their potential significance, only few studies have been carried out due to difficulties associated with laboratory measurements and numerical computations. In addition, the initiation mechanism of such cellular secondary currents has not yet been clearly demonstrated. The mutual interaction between the secondary currents and the sand bed is thought to be related to the initiation of cellular secondary currents. The presence of the free surface and sidewall as well as the non-uniformity of sediment particles is also known to strengthen the cellular secondary currents.

The purpose of this study is to investigate numerically the initiation mechanism of cellular secondary currents. The Reynolds averaged Navier-Stokes equations in curvilinear

coordinates are solved with the non-linear k-ε model. The developed model was applied to flows over a fixed sand ridges and troughs in order to check the performance of the model. The streamwise mean velocity and secondary currents are provided and comparisons are made with measured data in the literature. Then, the bed elevation changes are simulated in wide open-channel flows over sand bed by solving the Exner's equation. Changes in bed shear stress and bed elevation with time are also investigated.

2. MATHEMATICAL MODEL

Governing Equations

In order to simulate flows over longitudinal bedforms, the following transformation mapping the physical space onto a mathematical space is necessary:

$$x = x\ ;\quad \xi = \xi(y,z)\ ;\quad \eta = \eta(y,z) \tag{1a,b,c}$$

where (y, z) is the physical plane, (ξ, η) is the transformed plane, and x denotes the streamwise direction. Consider a steady open-channel flow at a high Reynolds number, and assume that the flow is uniform in the streamwise direction. Thus, the RANS equations in generalized curvilinear coordinates can be written as

continuity equation

$$\frac{1}{J}\left[\frac{\partial}{\partial\xi}\left(h_2 v^c\right)+\frac{\partial}{\partial\eta}\left(h_1 w^c\right)\right]=0 \tag{2}$$

streamwise momentum equation

$$\frac{v^c}{h_1}\frac{\partial u}{\partial\xi}+\frac{w^c}{h_2}\frac{\partial u}{\partial\eta}=-gS_0-\frac{1}{J}\left[\frac{\partial}{\partial\xi}\left(h_2\overline{u'v^{c\prime}}\right)+\frac{\partial}{\partial\eta}\left(h_1\overline{u'w^{c\prime}}\right)\right] \tag{3}$$

secondary-velocity-governing momentum equations

$$\begin{aligned}\frac{v^c}{h_1}\frac{\partial v^c}{\partial\xi}+\frac{w^c}{h_2}\frac{\partial v^c}{\partial\eta}+\frac{v^c w^c}{h_1 h_2}\frac{\partial h_1}{\partial\eta}-\frac{w^{c2}}{h_1 h_2}\frac{\partial h_2}{\partial\xi}&=-\frac{1}{\rho h_1}\frac{\partial p}{\partial\xi}\\ -\frac{1}{J}\left[\frac{\partial}{\partial\xi}\left(h_2\overline{v^{c\prime 2}}\right)+\frac{\partial}{\partial\eta}\left(h_1\overline{v^{c\prime}w^{c\prime}}\right)\right]&-\frac{\overline{v^{c\prime}w^{c\prime}}}{h_1 h_2}\frac{\partial h_1}{\partial\eta}+\frac{\overline{w^{c\prime 2}}}{h_1 h_2}\frac{\partial h_2}{\partial\xi}\end{aligned} \tag{4}$$

$$\begin{aligned}\frac{v^c}{h_1}\frac{\partial w^c}{\partial\xi}+\frac{w^c}{h_2}\frac{\partial w^c}{\partial\eta}+\frac{v^c w^c}{h_1 h_2}\frac{\partial h_1}{\partial\xi}-\frac{v^{c2}}{h_1 h_2}\frac{\partial h_2}{\partial\eta}&=-\frac{1}{\rho h_2}\frac{\partial p}{\partial\eta}\\ -\frac{1}{J}\left[\frac{\partial}{\partial\xi}\left(h_2\overline{v^{c\prime}w^{c\prime}}\right)+\frac{\partial}{\partial\eta}\left(h_1\overline{w^{c\prime 2}}\right)\right]&-\frac{\overline{v^{c\prime}w^{c\prime}}}{h_1 h_2}\frac{\partial h_2}{\partial\xi}+\frac{\overline{v^{c\prime 2}}}{h_1 h_2}\frac{\partial h_1}{\partial\eta}\end{aligned} \tag{5}$$

where v^c, and w^c are the streamwise, lateral, and vertical mean velocities in the transformed space, h_1 and h_2 are the coordinate transformation scale factors, J is the determinant of Jacobian, p is the pressure, ρ is the fluid density, g is the gravitational acceleration, and $\overline{u_i'u_j'}$ is the Reynolds stress.

Turbulence Model

The non-linear k-ε model by Speziale (1987) estimates the Reynolds stresses in Eqs.(3)-(5) using the following relationship:

$$-\overline{u_i' u_j'} = -\frac{2}{3}k\delta_{ij} + \frac{k^{5/2}}{\varepsilon}D_{ij} + C_D\frac{k^3}{\varepsilon^2}\left(D_{im}D_{mi} - \frac{1}{3}D_{mn}D_{nm}\delta_{ij}\right) + C_E\frac{k^3}{\varepsilon^2}\left(\dot{D}_{ij} - \frac{1}{3}\dot{D}_{mn}\delta_{ij}\right) \quad (6)$$

where k is the turbulent kinetic energy, ε is the dissipation rate of k, and C_D and C_E are dimensionless parameters. Speziale (1987) proposed C_D = C_E = 1.68 for internal flows without the free-surface effect. In Eq.(6), D_{ij} and $\dot{D}_{ij}$ are the strain tensor and the tensor of the frame-independent Oldroyd derivative of D_{ij}. They are, respectively, expressed as

$$D_{ij} = \frac{1}{2}\left(\frac{\partial u_i}{\partial x_j} + \frac{\partial u_j}{\partial x_i}\right); \quad \dot{D}_{ij} = \frac{\partial D_{ij}}{\partial t} + U\cdot\nabla D_{ij} - \frac{\partial u_i}{\partial x_k}D_{kj} - \frac{\partial u_j}{\partial x_k}D_{ki} \quad (7a,b)$$

In the present study, the finite volume method was used to discretize the transport equations, Eqs.(3)- (5). As the solution strategy, the SIMPLER algorithm proposed by Patankar and Spalding (1972) was employed. For the discretization of the convection and diffusion terms in the transport equations, the power-law differencing scheme by Patankar (1980) was used.

Exner's Equation

In order to estimate the bed elevation change, the following Exner's equation is solved:

$$(1-p')\frac{\partial z_b}{\partial t} + \frac{\partial q_{tx}}{\partial x} + \frac{\partial q_{ty}}{\partial y} = 0 \quad (8)$$

where p' is the porosity, q_t is bedload transport. In the present study, the following formula by Ashida and Michiue (1972) is used for the calculation of the bed load:

$$q^* = 17\left(\tau^* - \tau_c^*\right)\left[\left(\tau^*\right)^{1/2} - \left(\tau_c^*\right)^{1/2}\right] \quad (10)$$

where q^* is the dimensionless bed load transport rate ($=q_b/\sqrt{gRD_s}D_s$, here R= submerged specific gravity of the particle, D_s = sediment diameter), τ^* is the dimensionless shear stress, τ^* is the dimensionless critical shear stress (=0.05).

3. FIXED SAND RIDGES AND TROUGHS

The developed numerical model was applied to the experiments by Wang and Cheng (2006), in which they reported the mean flow data of an open-channel flow over longitudinal bedforms. The slope and the width of the channel were 0.0007 and 0.6 m, respectively. The flow depth was 0.075 m. The ridges were of wavy form, as shown in Figure 2, and their height was 11.7 mm.

Figure 3 shows the secondary current vectors. It can be seen that the developed numerical model successfully simulates pairs of counter-rotating secondary currents, i.e. upflows over the ridge and downflows over the trough. In alluvial rivers, this type of cellular secondary currents sweep out fine particles over the troughs and transport them to the ridges.

However, it was observed that the secondary currents towards the troughs were slightly weak compared with the measured data. This results in downflows over the troughs inclined to the top of the ridge.

Figure 4 shows the distribution of the streamwise mean velocity. The simulated results are normalized by the streamwise mean velocity at the center of the channel. It can be seen in this figure that the isovels are wavy in the transverse direction due to periodic changes of bed elevation. That is, the mean velocity over the trough is larger than that over the ridge. This is because the downflows over the trough converct the high momentum fluids near the free surface toward the bottom. Similarly, the simulated profile shows that the maximum streamwise velocity occurs over the trough.

Figure 5 shows contour plots of the normalized vertical mean velocity. It can be seen that the numerical model reproduced the overall magnitude of the upflows. However, the computed vertical mean velocity over the trough was underestimated compared with the measured data.

4. BED ELEVATION CHANGES

The bed elevation changes are simulated in wide rectangular channel flows over a mobile bed. The computations are based on the decoupled modelling approach assuming that the interaction between flow and bed is ignorable during the computational time step. Also, the model is restricted to beds of uniform sediment without armouring or grain sorting effects. The computational conditions are a water depth of 0.04 m, a channel width of 0.3 m, a bottom slope of 0.00152, and a sediment diameter of 75μ.

Figure 6 shows the time variations of the bed elevation changes and secondary currents. In this figure, the contour plot depicts the streamwise mean velocity. For the initial rectangular channel flow, as seen in Figure 6(a), two pairs of counter-rotating vortices comprised of the free surface vortex and the bottom vortex are observed. At t = 10 sec, it appears that the bottom is firstly eroded near the sidewall due to the strong downflow of the corner vortex. On the contrary, in the region away from the sidewall, the eroded sediment near the sidewall is laterally transported and deposited due to the bottom vortex. The pattern of sediment erosion and deposition becomes to be clear with time. When t = 150 sec, the initial flat bed becomes longitudinal bedforms composed of ridges and troughs. Also, it appears that the isovels are wavy in the transverse direction due to the secondary currents.

Figure 7(a) shows the pattern of secondary currents made over the longitudinal bedforms when t = 150 sec. It can be seen in this figure that pairs of counter-rotating vortices occur over the entire cross section and upflows and downflows occur over the ridges and the troughs, respectively. Figure 7(b) shows the transverse distribution of the bottom shear stress. In this figure, the bottom shear stress is normalized by its mean value and the arrows depict the direction of cellular secondary current vectors. The bottom shear stress shows wavy form. The bottom shear stress over the ridge is found to be smaller than that over the trough. This is caused by the cellular secondary currents. That is, the downflow over the trough transfer high momentum from the free surface toward the bottom.

Figure 8 shows the changes of the bottom shear stress with time. The bottom shear stress in the initial bed increases from the sidewall and shows a local minimum at about y = 0.08 m. Then, the bottom shear stress increases again and becomes nearly a constant in the central region. The local minimum of the bottom shear stress corresponds to the upflow of the bottom vortex. This inflection point of the bottom shear stress causes the sediment transport to vary in the spanwise direction, and as a result, longitudinal bedforms may be produced. The bottom shear stress becomes wavy with time, and when t = 150 sec, 3 inflection points was

observed.

5. CONCLUSIONS

In this study, the initiation mechanism of cellular secondary currents was numerically investigated. For flow, the time-averaged Navier-Stokes equations, closed by the non-linear k-ε model, were solved. For bed elevation change, the Exner's equation was employed.

The developed model was applied to flows over a fixed sand ridges and troughs in order to check the performance of the model. The simulated results are compared with experimental data available in the literature. The simulated pattern of cellular secondary currents was found to be consistent with the observed data, showing upflows and downflows over ridges and troughs, respectively. Next, the bed elevation changes were simulated in wide rectangular open-channel flows over uniform sediment bed by solving the Exner's equation. The simulated results showed that the bottom is firstly eroded near the sidewall due to the strong downflow of the corner vortex. In the region away from the sidewall, the eroded sediment near the sidewall is laterally transported and deposited. It is due to the lateral flow of the bottom vortex. The initial flat bed was found to be gradually deformed, and finally became ridges and troughs. The inflection point in the initial bed was observed and this is an important cause of initiation mechanism of cellular secondary currents.

REFERENCES

Allen, J.R.L. (1984). *Sedimentary Structure*, vol. 2, Elsevier, New York, NY.

Ashida, K. and Michiue, M. (1972). "Study on hydraulic resistance and bed load transport rate in alluvial streams." *Transactions of the Japan Society of Civil Engineering*, 206, 59-69.

Culbertson, J.K. (1967). "Evidence of secondary circulation in an alluvial channel." *U.S. Survey Prof. Paper*, 575-D, 214-216.

Nezu, I. and Nakagawa, H. (1993). *Turbulence in open-channel flows*. IAHR Monograph, A.A. Balkema, The Netherland.

Karcz, I. (1966). "Secondary currents and the configuration of a nature stream bed." *Journal of geophysical Research*, 71, 3109-3116.

Kinoshita, R. (1967). "An analysis of the movement of flood waters by aerial photography; concerning characteristics of turbulence and surface flow." *Photographic Surveying*, 6, 1-17 (in Japanese).

Patankar, S.V. (1980). *Numerical Heat Transfer and Fluid Flow*, Hemisphere Publishing Corporation, Taylor & Francis Group, New York.

Patankar, S.V. and Spalding, D.B. (1972). "A calculation procedure for heat, mass and momentum transfer in three dimensional parabolic flows." *International Journal of Heat and Mass Transfer*, 15(10), 1787-1806.

Speziale, C.G. (1987). "On non-linear k-l and k-ε models of turbulence." *Journal of Fluid Mechanics*, 178, 459-475.

Vanoni, V.A. (1946). "Transportation of suspended sediment by water." *Transaction of ASCE*, ASCE, 111, 67-133.

Wang, Z.-Q. And Cheng, N.-S. (2006). "Time-mean structure of secondary flows in open channel with longitudinal bedforms" *Advances in Water Resources*, 29, 1634-1649.

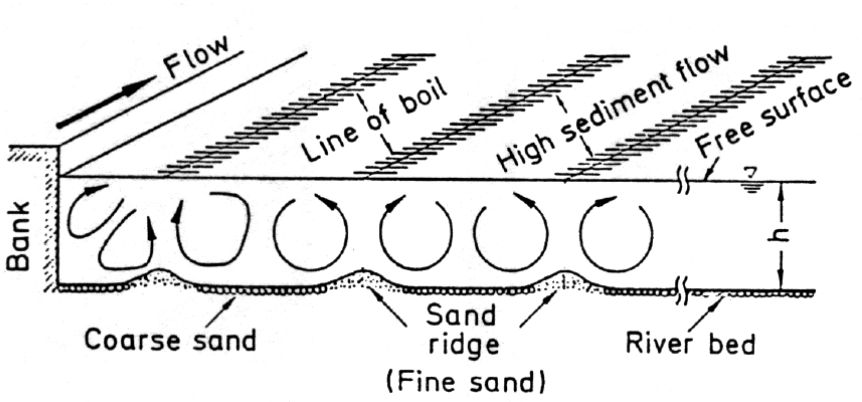

Figure 1. Schematic sketch of cellular secondary currents (Nezu and Nakagawa, 1993)

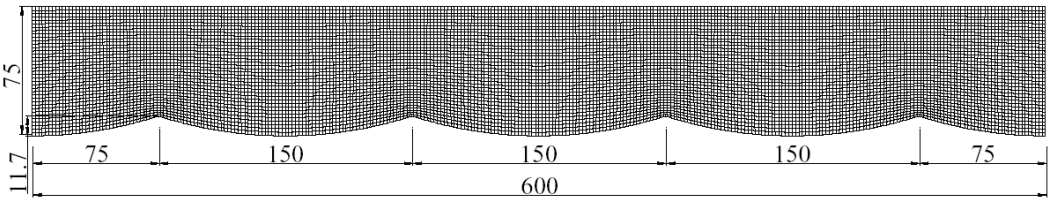

Figure 2. Solution domain and grid arrangement (unit: mm)

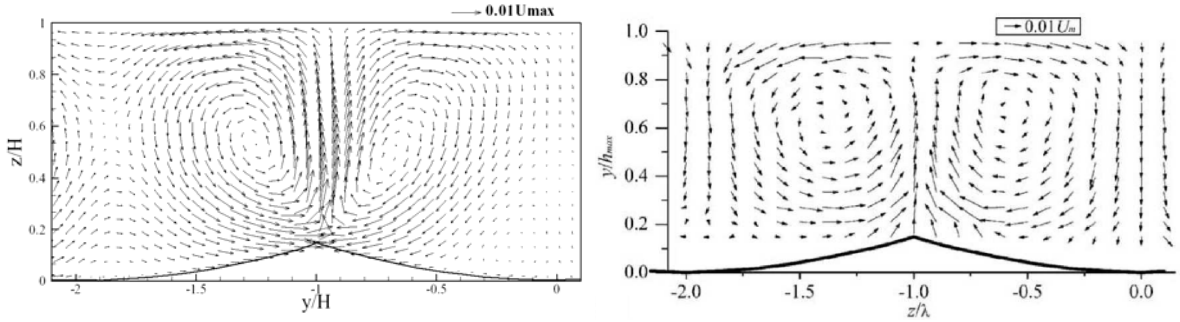

(a) Non-linear k-ε model (b) Wang and Cheng (2006)

Figure 3. Cellular secondary currents

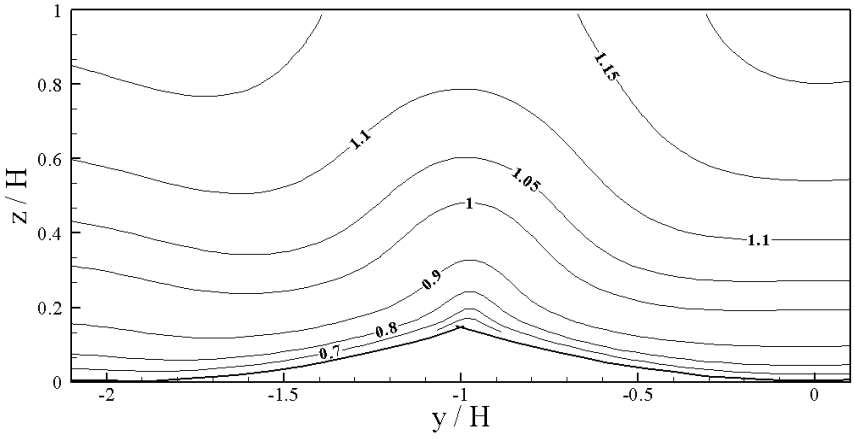

Figure 4. Streamwise mean velocity ($\bar{u}/U_m$)

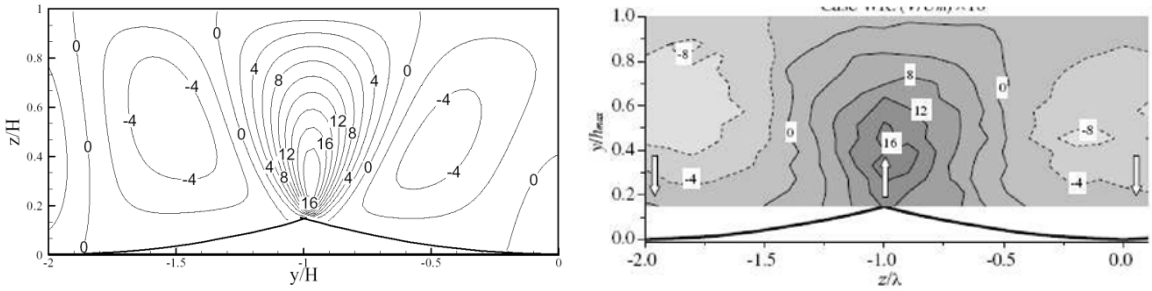

(a) Non-linear k-ε model (b) Wang and Cheng (2006)

Figure 5. Vertical mean velocity ($\overline{w}/U_m \times 10^3$)

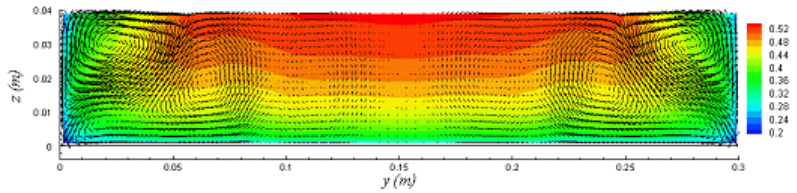

(a) t = 0

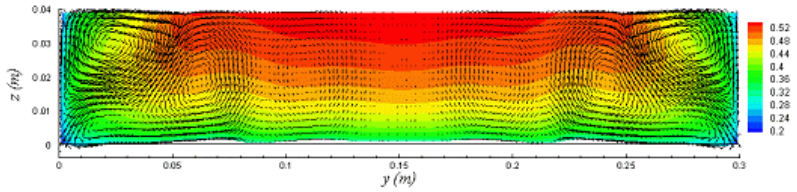

(b) t = 10 sec

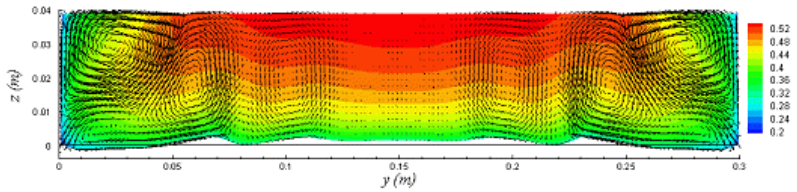

(c) t = 50 sec

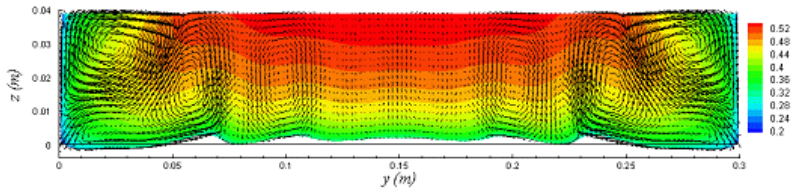

(d) t = 100 sec

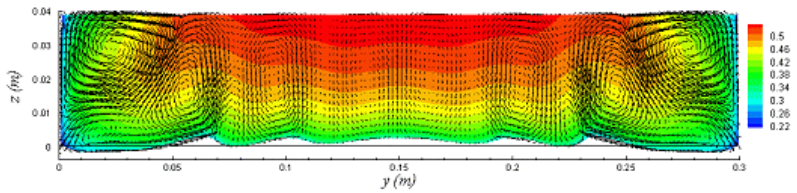

(e) t = 150 sec

Figure 6. Bed elevation changes with time

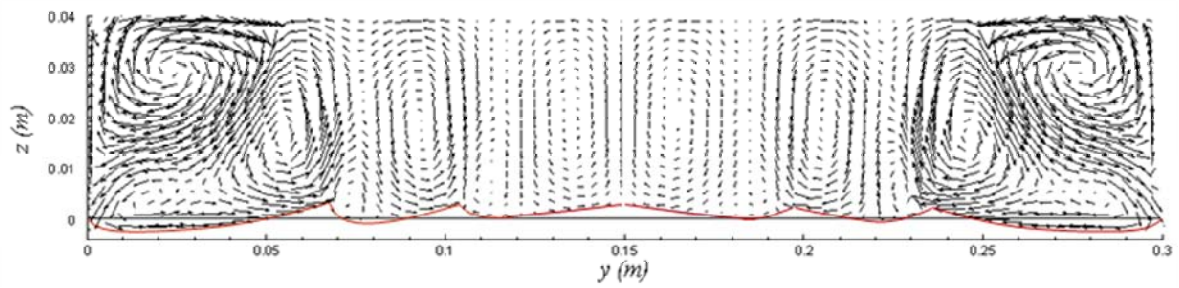

(a) cellular secondary currents

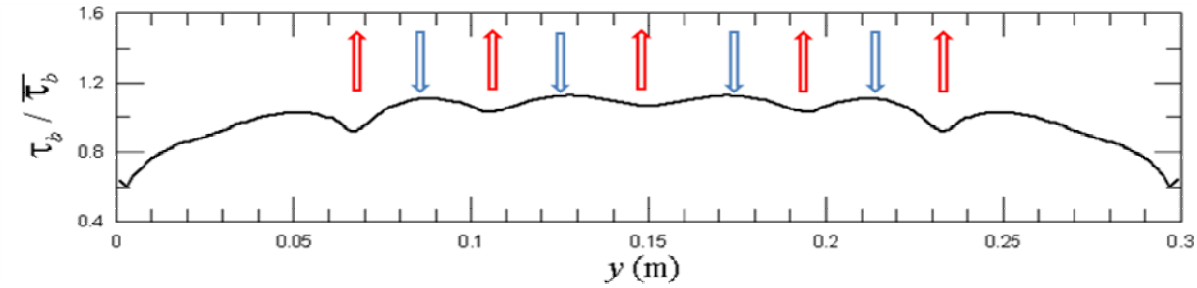

(b) bed shear stress

Figure 7. Cellular secondary currents and bed shear stress at t = 150 sec

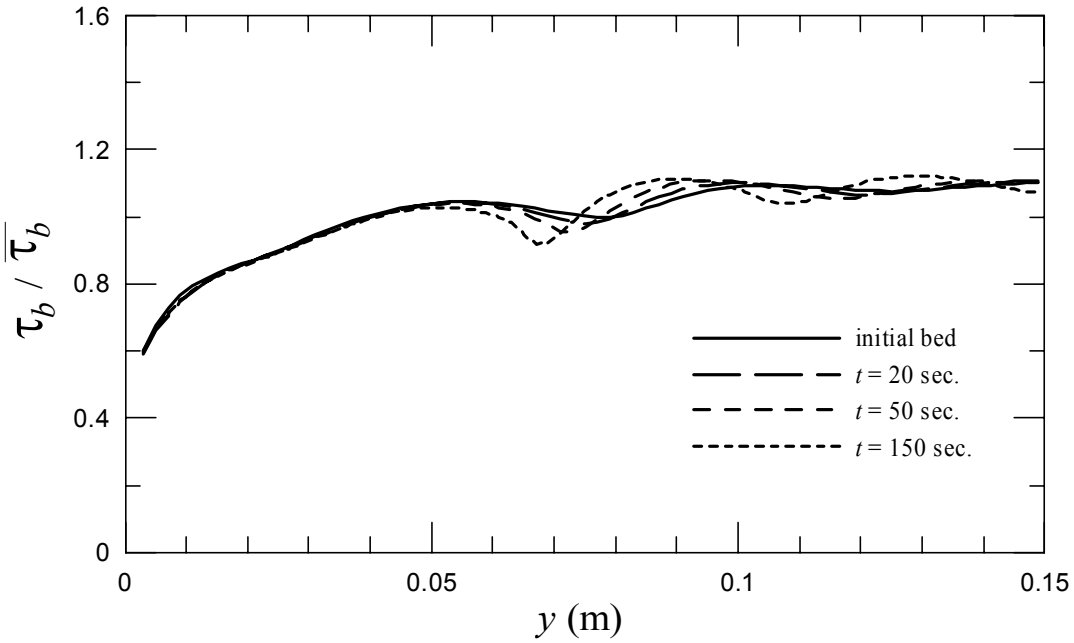

Figure 8. Changes the bottom shear stress with time